A widely applicable strategy to convert fabrics into lithiophilic textile current collector for dendrite-free and high-rate capable lithium metal anode

Ruijie Zhu,[a] *Chunyu Zhu* [a,b] * *Nan Sheng,* [b] *Zhonghao Rao,*[b] *Yoshitaka Aoki,*[a] *Hiroki Habazaki* [a]

[a] Faculty of Engineering, Hokkaido University, Sapporo 060-8628, Japan.

[b] Jiangsu Province Engineering Laboratory of High Efficient Energy Storage Technology and Equipments & School of Electrical and Power Engineering, China University of Mining and Technology, Xuzhou, 221116, China

Corresponding Author

* E-mail: chunyu6zhu@eng.hokudai.ac.jp

ABSTRACT Hindered by dendrite growth, unceasing volume change and repeated regeneration of solid-state interface, the practical application of lithium (Li) metal anode is still facing challenges from low Coulombic efficiency (CE), insufficient safety performance and poor cyclic stability. Current collector plays a key role in regulating Li deposition and suppressing dendrite growth. In this report, through a simple bio-template method, a textile-structured nickel (Ni) framework is fabricated as current collector for Li metal anode, whose unique micro-nano hierarchical structure is adequate for accommodating Li. A good performance after more than 200 cycles at 3 mA cm^{-2} during repeated Li plating/stripping is remained in virtue of this unique structure design. By further introducing Ag_2S nanoparticles uniformly to the current collector, a dendrite-free and high reversible Li metal anode is achieved, showing low over-potential (~24 mV at 1 mA cm^{-2}), high CE (~98%) and excellent quick charging/discharging stability (up to 350

cycles at 10 mA cm^{-2} in symmetric cell). Furthermore, this new strategy for constructing textile-structured metallic framework opens a foreground for various applications of porous metals.

KEYWORDS Lithium metal anode, Li metal battery, textile structure, bio-template, metallic current collector.

1. Introduction

Lithium (Li) metal has been considered as one of the most promising anode materials for rechargeable Li-based batteries, such as Li-O_2 battery and Li-S battery, because of its ultrahigh theoretical capacity (3860 mA h g^{-1}), lowest negative potential (-3.040 V vs the standard hydrogen electrode) and a low mass density (0.53 g cm^{-3}) [1-3]. However, the practical utilization of Li metal anode is hindered by two pivotal problems: i) dendritic Li growth due to the inhomogeneous Li deposition; ii) unceasing side reactions induced by the thermodynamically unstable interface between Li and electrolyte. Those will lead to the disastrous consequences for Li metal batteries, including the increasing of internal resistance, low Coulombic efficiency (CE) and hazard of short circuit [4,5].

In the past several years, considerable efforts have been devoted to enhancing the cycling stability of Li metal anode by employing a variety of strategies. In one approach, due to the fact that the protogenous solid-state electrolyte interface (SEI) on Li metal is always heterogeneous and fragile, stable artificial SEI layers with high conductivity, such as lithium nitride (Li_3N) or lithium sulfide (Li_2S), were pre-coated onto Li metal, and the significantly stabilized electrochemical behavior has been confirmed by several groups [6-13]. However, the irregular deposition of Li still occurs underneath the SEI which inevitably deteriorates the electrode

performance as the cycling proceeds. The initial nucleation of dendritic Li is correlated to both the Li ion migration rate and the effective electrode current density, which is depicted as the diffusion model called "Sand's Time" [14, 15]. In addition, the growth rate of dendritic Li is determined by Li ion migration direction and rate [16]. Therefore, a three-dimensional (3D) porous current collector with large surface area will decrease the local current density and inhibit the formation of Li dendrite [17-19]. In particular, the hierarchically micro-nano structured 3D current collector, which can disperse the electronic field and Li-ion flux simultaneously, is efficient for regularizing the electrodeposition behavior of Li and alleviating the dendritic Li growth [20-23].

Considering that metallic nickel (Ni) and copper (Cu) own good electronic conductivity and high mechanical strength, they are suitable current collector which have been widely used in commercial batteries. However, as a 3D container to incorporate Li metal, Ni/Cu framework is not lithiophilic to reduce the severe Li nucleation over potential, resulting in non-uniform plating of Li nuclei [24, 25], thus Li metal cannot be infiltrated into the interior of the porous current collector. In addition, the pathway of Li ion migration can be gradually blocked by previously deposited Li on the surface and the subsequent Li deposition can only proceed on the top of the 3D current collector, especially when a high deposition capacity is involved, making insufficient utilization of the 3D porous structure [20, 26, 27]. For this reason, most of the currently reported metallic 3D current collectors can only work stably for less than 250 cycles at a low current density and a low deposition capacity, *i.e.,* $\leq$ 1 mA cm^{-2} and $\leq$ 1 mA h cm^{-2} [21, 27-29]. Zhao et. al. developed a 3D Cu current collector through an electrochemical dealloying strategy, and a stable Li plating/stripping performance was observed up to 200 cycles at 1 mA cm^{-2} to a capacity of 1 mA h cm^{-2} [30]. Zhang and his co-workers pre-stored Li into a 3D Ni foam, and stable cycle performance could be maintained more than 100 cycles at 5 mA cm^{-2} to a capacity of 1 mA h cm^{-}

^{2} [31]. Even with additional decoration strategies applying to the metallic 3D current collectors, such as modifying Ni foam with lithiophilic Ni nitrides layer (illustrating a tested performance up to 160 cycles at 5 mA cm^{-2} to 1 mAh cm^{-2}) [32] or constructing a lithiophilic Cu-CuO-Ni hybrid 3D structure (with a tested performance up to 300 cycles at 1 mA cm^{-2} to 1 mA h cm^{-2}) [33], the cycle performance is still unsatisfying, especially when the cells were cycling at high current densities.

Employing cellulose based materials as templates for developing bio-inspired materials is regarded as an efficient and convenient strategy [23, 34-38]. Herein, we develop a simple cotton fabric template method to produce 3D metallic current collector with textile structure for Li metal anode. By using the cotton canvas template method, the canvas structured Ni current collector (Canvas Ni) is obtained. When the hierarchically micro-nano porous Canvas Ni is used for accommodating Li metal, a performance that is far superior to previously reported 3D metallic current collectors is observed, *i.e.,* > 200 cycles at 3 mA cm^{-2} with a capacity of 1 mA h cm^{-2}. With further decoration with lithiophilic Ag_2S nanoparticles (NPs) to the metallic framework, a stable cycle performance under high current density is observed (up to 350 cycles at 10 mA cm^{-2} to 1 mA h cm^{-2}), which is rarely reported in literatures for Li metal anode using 3D metallic current collectors.

2. Experimental Section

2.1. Preparation of Canvas Ni framework

A piece of cotton canvas fabric (size 7.0 cm×2.5 cm) was firstly cleaned in acetone by consecutive ultrasonication for 30 min and then dried in vacuum oven. Nickel acetate tetrahydrate ($Ni(CH_3COO)_2 \cdot 4H_2O$, Labchem-Wako) was dissolved in ammonia solution with a concentration of 28% ~ 30% (Kanto Chemical) to prepare a 2.5 mol L^{-1} Ni source solution. The dried cotton fabric was firstly soaked in the Ni source solution for 12 h, followed by calcining at 600 ℃ for 2 h in air to remove the cotton fabric template. The as-prepared Canvas NiO precursor was subsequently reduced by hydrogen gas in a tubular reactor at 650 ℃ for 1 h to obtain the Canvas Ni framework. The optimized production condition of using 2.5 mol L^{-1} Ni solution is shown in **Fig. S**16.

2.2. Preparation of Ag_2S nanoparticles coated Canvas Ni electrode

A silver mirror reaction was used to deposit Ag nanoparticles on the Canvas Ni electrode. An ammonia solution which contained 6.375×10^{-3} mol L^{-1} silver nitrate ($AgNO_3$, Labchem-Wako, 99.8%), 3.405×10^{-2} mol L^{-1} glucose ($C_6H_{12}O_6$, Kanto Chemical, 98%) and 4.005×10^{-3} mol L^{-1} tartaric acid ($C_4H_6O_6$, Kanto Chemical, 99.5%) was used as the silver mirror reagent. The Canvas Ni electrode was soaked in the freshly prepared silver mirror reagent for 30 min. In this way, Ag nanoparticles were formed on the Canvas Ni, which was subsequently washed by ethanol/deionized water for several times and dried in a vacuum oven. The determination of a reaction time of 30 min is shown in **Fig. S**17.

Dimethyl sulfoxide (DMSO, Kanto Chemical, 99%) which contained 2×10^{-2} mol L^{-1} sulfur was used as the sulfurization reagent. The Ag nanoparticles coated Canvas Ni was put into the sulfurization reagent and kept at 100 °C for 1 h. The Ag_2S coated Canvas Ni electrode was washed

by toluene and deionized water carefully afterward, which was finally dried in a vacuum oven at 100 ℃ for 24 h.

2.3. Electrochemical Measurements

To investigate the electrochemical deposition behavior and the Coulombic Efficiency of Li stripping/plating on different electrodes, a half-cell measurement in a Swagelok cell was conducted with a Li planar foil (Alfa Aesar, 99.9%) as the counter/reference electrode and the Canvas Ni-Ag_2S electrode with a 10 mm disk shape or Canvas Ni electrode or planar Cu foil (as control group) as the working electrode.

To investigate the voltage hysteresis during long-term plating/stripping process, we firstly deposited 8 mA h cm^{-2} of Li onto the Canvas Ni-Ag_2S electrode or Canvas Ni electrode at a current density of 1 mA cm^{-2} in a Swagelok cell to prepare Li@Canvas Ni-Ag_2S electrode or Li@Canvas Ni electrode. The pre-plated electrodes were taking out from the cells and washed with 1,2-dimethoxyethane (DME). Symmetrical cells were assembled with two identical Li@Canvas Ni-Ag_2S electrodes or Li@Canvas Ni electrodes or Li planar foils (as control group).

All of the mentioned cells in this paper were assembled/disassembled in an argon filled glovebox. The galvanostatic discharge-charge cycle performance was carried out on a multi-channel battery tester (Hokuto Denko). The electrolyte was 1 mol L^{-1} lithium bis(trifluoromethanesulfonyl)imide (LiTFSI, Kishida Chemical, 99.90%) and 1 wt% lithium nitrate ($LiNO_3$, Kanto Chemical) in a mixed solution of 1,3-dioxolane (Sigma-Aldrich, 99.8%) and 1,2-dimethoxyethane (Sigma-Aldrich 99.5%) (DOL/DME, 1:1 v/v). Dosage of electrolyte

used in each cell was 125 μL. A glass fiber separator was placed between two electrodes. In order to remove the surface contaminations and make the electrodes contain the same areal capacity of Li metal, the half-cell measurement was first cycled at 0-1 V versus Li at 50 μA for six cycles. The pre-plating process started when the voltage dropped to 0 V at the sixth discharge step. The cut off voltage was set to 1 V for Li stripping process and -2 V for Li plating process.

To investigate the impedance change during long-term plating/stripping process, Li foil | Li foil, Canvas Ni | Li@Canvas Ni, and Canvas Ni-Ag_2S | Li@Canvas Ni-Ag_2S cells were assembled. Here, the Li foil, Canvas Ni and Canvas Ni-Ag_2S were used as the working electrodes. Li was firstly plated onto the working electrodes to a controlled capacity of 4 mA h cm^{-2} at 1 mA cm^{-2}. In this way, the cells were changed to symmetric cells, which were subsequently cycled for repeated plating/stripping at 1 mA cm^{-2} with a capacity of 1 mA h cm^{-2}. The electrochemical impedance spectra (EIS) at different cycles were obtained by a Princeton apparatus (Princeton VersaSTAT 3) with a frequency range of 100 kHz to 0.1 Hz.

To evaluate the performance of full cells, lithium cobalt oxide ($LiCoO_2$) was employed as cathode, while Li@Canvas Ni-Ag_2S electrode or Li@Canvas Ni electrode or Li planar foil was used as anode. $LiCoO_2$ slurry was prepared by mixing the active material, *poly-vinylidene difluoride* (PVDF) binder and carbon black with a weight ratio of 8:1:1 in *N*-methyl-2-pyrrolidone (NMP) (Chameleon Reagent, LBG-50481). After pasting the slurry to an Al foil, the $LiCoO_2$ cathode was dried at room temperature for 2 h and 110 ℃ for 12 h in a vacuum oven. The areal mass load on the Al foil current collector for the cathode with a disk size of 10 mm was 2.5 mg cm^{-2}. The electrolyte used was the binary carbonate solution which contained 1 mol L^{-1} $LiPF_6$ in ethylene carbonate/dimethyl carbonate (EC/DMC 1:1 v: v) (Chameleon Reagent, LBG-00022). Dosage of electrolyte used in each cell was 100 μL and the separator used in all cells was glass

fiber. The galvanostatic charge/discharge measurement was conducted in the voltage range of 3.0 V~ 4.2 V for the full cells. The specific capacity of discharge was calculated based on the mass of active material.

2.4. Materials characterization

Morphologies of the samples were characterized by a scanning electron microscope (SEM, ZEISS Sigma 500). The Li composite electrodes after electrochemical test at different status were firstly taken out from the cells and rinsed by DOL/DME to remove the residue of electrolyte. After drying in the glovebox, the electrodes were kept in Ar-filled containers for further ex-SEM or ex-XPS observation. Crystal structures of the materials were measured by X-ray diffractometer (XRD, Rigaku MiniFlex600) using Cu Kα radiation. Energy dispersive spectroscopy (EDS) characterized by a scanning electron microscope (SEM, JSM-7500F, JEOL) was also performed on the current collector to confirm the chemical composition. X-ray photoelectron spectroscopy (XPS) measurement were conducted by using an Al-Kα X-ray source (JEOL, JPS-9200). The Brunauer-Emmett-Teller (BET) specific surface area and the Barrette-Joynere-Halenda (BJH) pore size distribution of the porous frameworks were characterized on a nitrogen adsorption surface area analyzer (BELSORP-mini).

3. Results and discussion

As shown in **Fig. 1**a, through a series of treatments, including immersion of Ni source to cotton canvas fabric, calcination under air to remove the canvas template and reduction under

hydrogen, metallic Canvas Ni was obtained which can preserve the original canvas textile structure. Afterward, uniform deposition of Ag NPs on the Ni substrate was achieved by a silver mirror reaction, and subsequently Ag NPs were sulfurized in a DMSO solution containing sulfur to form Ag_2S NPs decorated Canvas Ni (named as Canvas Ni-Ag_2S). The Canvas Ni framework is served as a 3D current collector with high mechanical strength and high electronic conductivity for accommodating Li. The porous structure allows the 3D current collector to have a weight even lower than Cu foil (see **Table S1**), indicating that this kind of material has a large potential in developing high energy density batteries. The presence of Ag_2S NPs not only act as lithophilic sites for inducing Li deposition into the interior pores of 3D current collector, but also act as a precursor for generating artificial Li_2S SEI. As depicted in **Fig. 1**b, Canvas Ni-Ag_2S electrode shows mainly three advantages: i) the enlarged surface area and the hierarchical micro-nano porous structure of Ni skeleton can effectively decrease the local current density (as shown **Fig. S1**); ii) the Ag_2S NPs can guide homogeneous Li nucleation and prevent dendrite growth of Li; iii) the 3D and hierarchically porous Canvas Ni framework can provide adequate space to alleviate the huge volume change during Li plating/stripping. These characteristics finally ensure the Li anode with a stabilized and long cycle performance at a high current density.

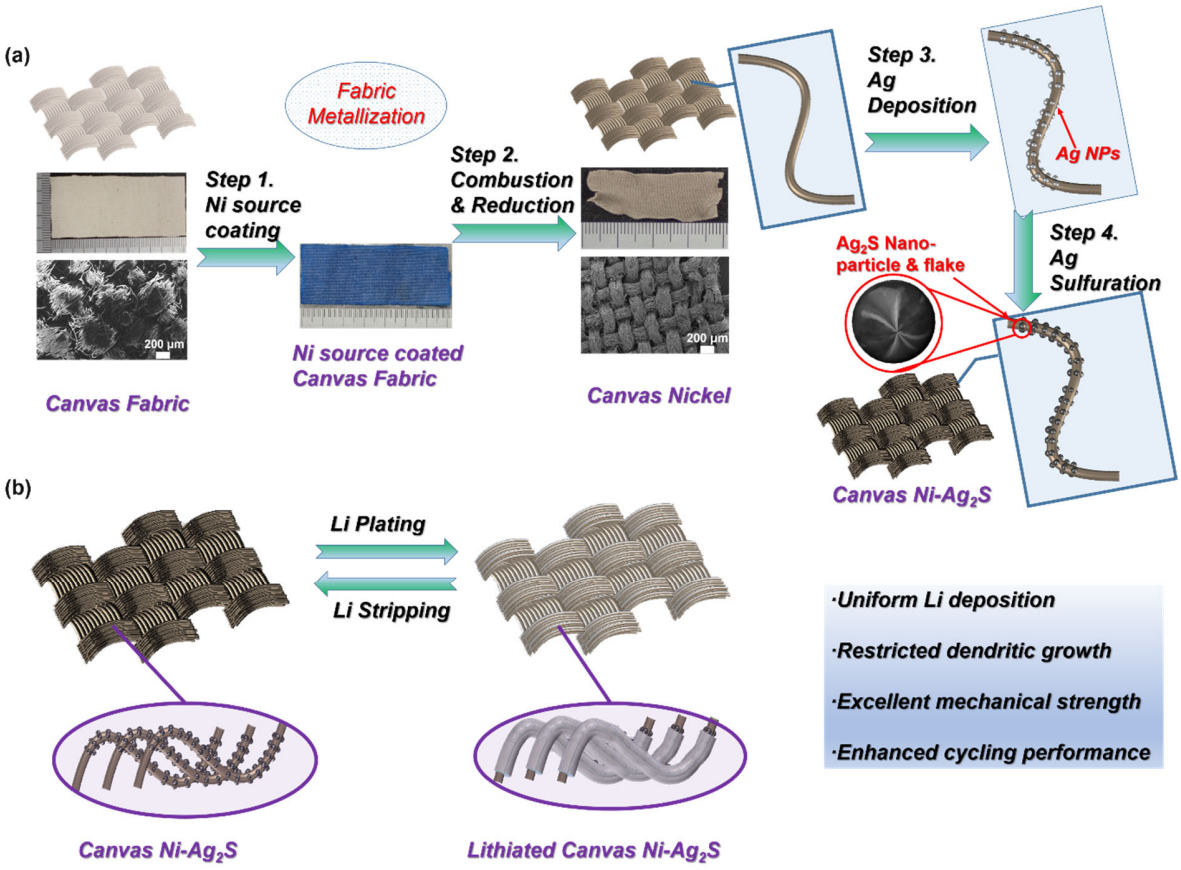

Fig. 1. (a) Scheme of the preparation of Canvas-Ni and Canvas Ni-Ag_2S frameworks. Optical photos of the fabric template and the Canvas Ni are included. (b) Graphical representation of the uniform electrodeposition behavior of Li on the Canvas Ni-Ag_2S electrode during plating and stripping.

Scanning electron microscope (SEM) images and optical photos of the Canvas Ni disk electrode are presented in **Fig. 2**a-c, and it is worth mentioning that the Canvas Ni is flexible. Similar to the morphology of canvas fabric, metallic Ni fibers are converged to form a "bundle", which lefts a plenty of voids inside. Careful observation of a single metallic fiber indicates that the fiber is porous containing pores of around 1 μm. More SEM images at different scales are also shown in **Fig. S3**. As previously reported, this pore size is suitable for Li deposition [28]. By a modified silver mirror reaction [39], Ag NPs are evenly deposited onto the surface of Ni fibers through the entire Canvas Ni to form the Ag NPs coated Canvas Ni. After deposition of Ag NPs, color of the Canvas Ni disk changes from gray to silver white (**Fig. 2**c and **Fig. 2**f). The SEM images are shown in **Fig. 2**d,e and **Fig. S4**. There are no structure changes of the textile skeleton except the coating of Ag NPs on Ni fibers, indicating that the destruction of the active Ni substrate by the replacement reaction between Ni and Ag^+ can be avoided through our modified silver mirror reaction. Finally, the Ag NPs are transformed to Ag_2S through a mild sulfurization strategy. The color of the disk electrode changes to black after sulfurization treatment (**Fig. 2**i). The textile structure is well retained and the Ag_2S NPs are constructed with nanoflakes, as shown by the SEM images in **Fig. 2**g,h and **Fig. S5**. The composition analysis by X-ray diffraction (XRD) of the Canvas electrodes treated at different stages is shown in **Fig. S6**, confirming the formation of targeted substances at each step. Energy dispersion spectroscopy (EDS) analysis results of the Canvas Ni (**Fig. S7**) treated by the same sulfurization solution in comparison with EDS results of Canvas Ni-Ag (**Fig. S8**) and Canvas Ni-Ag_2S (**Fig. S9**) confirm that the mild sulfurization reaction is only performed on Ag NPs.

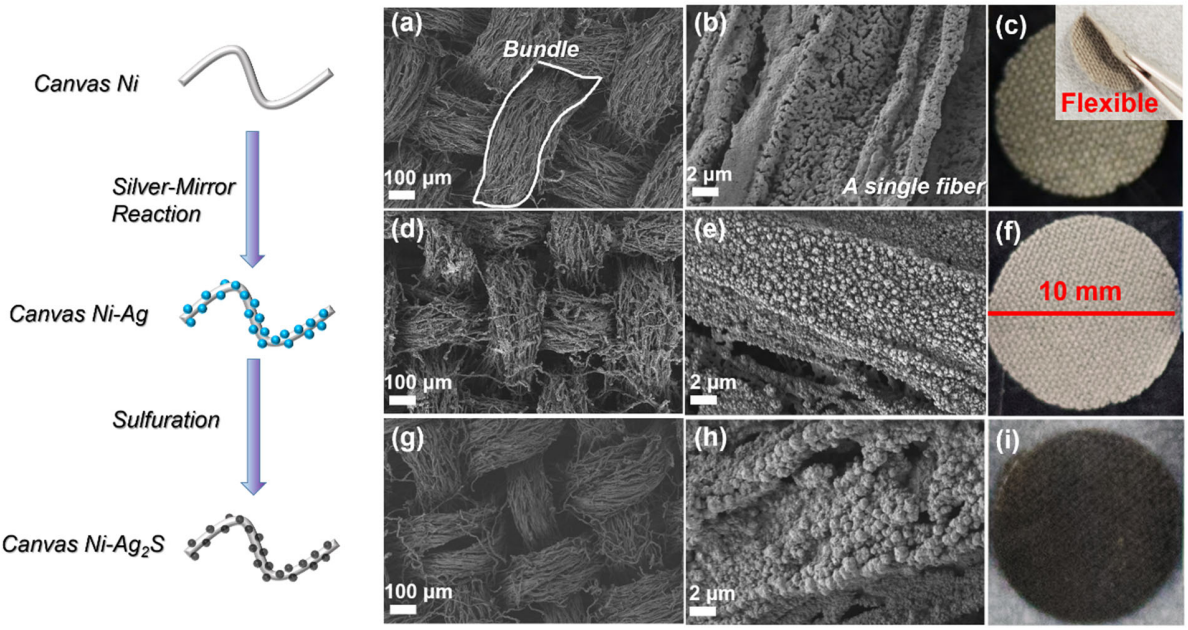

Fig. 2. SEM images and optical images for the textile electrode treated at different stages. a,b,c) as-prepared Canvas Ni electrode, d,e,f) Canvas Ni-Ag and g,hi) Canvas Ni-Ag_2S. The inset in Fig. 2c is the optical photo for showing the flexibility of Canvas Ni electrode.

To preliminarily estimate whether the obtained materials are suitable for Li metal anode, the electrodeposition behavior of Li on Canvas Ni, Canvas Ni-Ag_2S and planar Cu foil were investigated, respectively. Li was firstly electrodeposited to an areal capacity of 1 mA h cm^{-2} at a current density of 1 mA cm^{-2} onto those electrodes after SEI formation pre-treatment, and the morphologies of the Li pre-plated electrodes were captured by SEM. As can be seen in **Fig. 3**a, most of the Li metal is deposited on the current collector to form a flat surface, and spherical Li crystals are deposited around the Ni fibers of the Canvas Ni substrate (**Fig. 3**b and 3c), indicating that the 3D porous Canvas Ni current collector is useful to store Li. However, due to the lack of lithiophilicity for the pure Ni substrate, dendritic Li with a "whisker growth mode" is also observed (**Fig. 3**a) which suggests a high over-potential of Li nucleation on the bare metallic current collector [40]. The as-grown Li dendrites can be merged together and are confined within the spaces and voids among Ni bundles and fibers (**Fig. 3**a), leading to the flat surface morphology on the Canvas Ni electrode (**Fig. 3**d). The nucleation of Li crystals is preferred on the surface side of the bare current collector. As the growth of Li crystals, the diffusion pathway for Li^+ is obstructed by the previously deposited Li crystals near the surface, therefore, the continuing Li deposition can only proceed at the top surface of Canvas Ni (**Fig. 3**e and **Fig. 3**f). Therefore, a lithiophilic surface treatment of the Ni substrate is needed to lead the deposition of Li inside the porous electrode. It is also noted that the dendritic Li crystals mainly form at the edges of Ni fiber bundles. This is because of that the top of the electrode is compressed by the separator, hence the dendrites are spread to the spaces between bundles [41]. As a result, the growth of Li crystals can be restricted inside the porous structure, preventing the quick piercing of the separator, which is one

advantage of the 3D current collector, particularly, that our textile electrodes have multi-scaled pores.

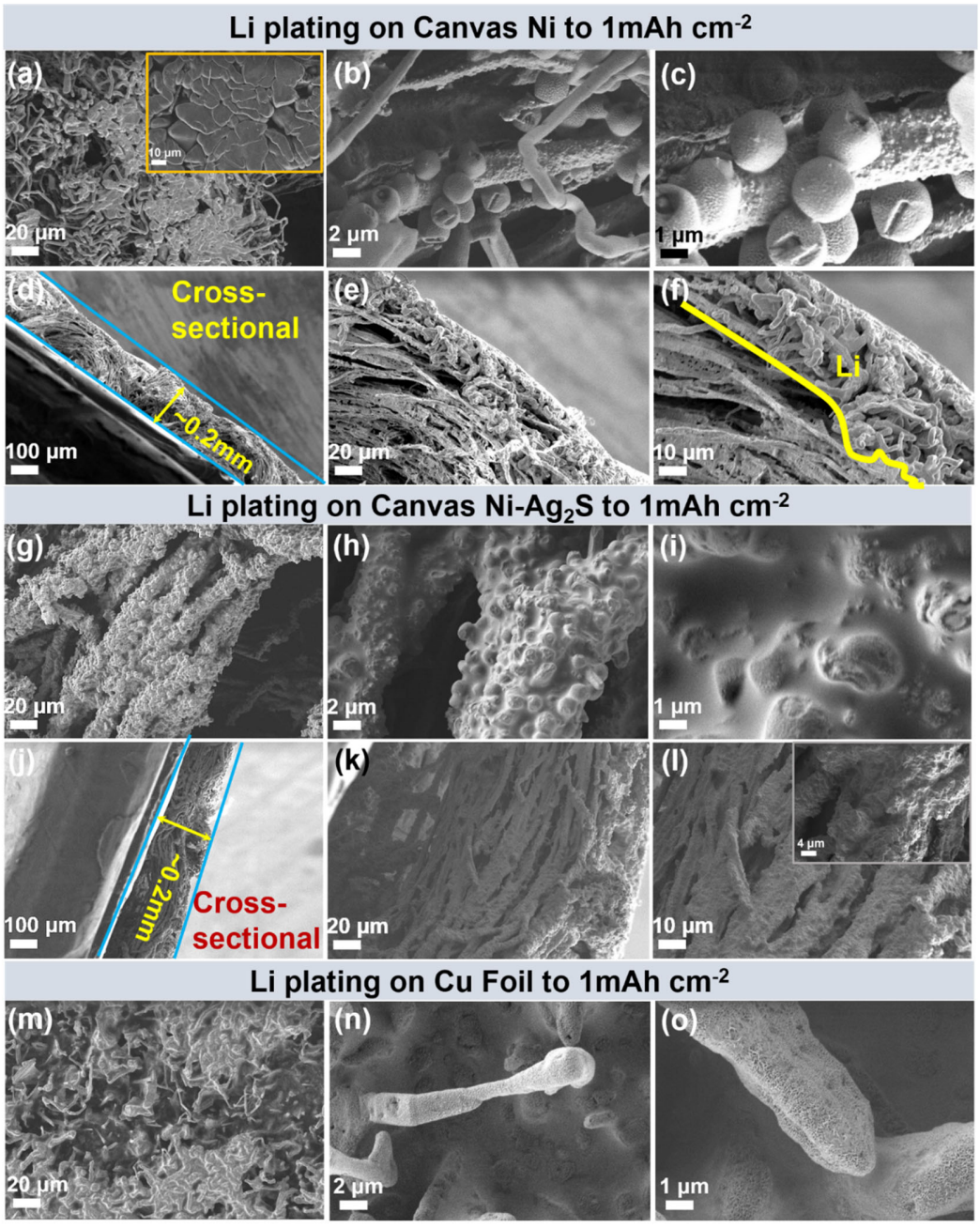

Fig. 3. SEM images of the Li electrodeposition behavior on different electrodes. a-c) Top view and d-f) cross-sectional observation for the Canvas Ni after Li plating to a restricted capacity of 1

mA h cm $^{-2}$. g-i) Top view and j-l) cross-sectional observation for the Canvas Ni-Ag_2S after Li plating to a restricted capacity of 1 mA h cm $^{-2}$. m-o) Li dendrites on Cu foil after Li plating to 1 mA h cm^{-2}.

The Li deposition behavior in the porous electrode can be greatly improved by further introducing lithiophilic substances (Ag_2S) on Ni surface. The low magnification SEM image (**Fig. 3**g) of lithiated Canvas Ni-Ag_2S electrode indicates a dendrite-free morphology. For the Canvas Ni-Ag_2S electrode, Ag_2S NPs are homogeneously covered on the surface of the Ni fibers. Two reactions occur during the initial pre-SEI process in the potential range of 0-2 V vs. Li (**Fig. S10**b):

$$Ag_2S + 2\,Li \longrightarrow 2\,Ag + Li_2S \qquad (1)$$

$$Ag + Li \longrightarrow Ag\text{-}Li\ (alloy) \qquad (2)$$

The conversion reaction between Ag_2S and Li at around 2 V induces the formation of Li_2S, which can be observed in XPS spectra of the S 2p species and the Li 1s species shown in **Fig. S11**a. It is regarded that Li_2S is a good SEI component for Li metal anode. [11, 42] The following potential plateau near 0 V is the alloying reaction between Ag and Li. After the stabilization of SEI layer, Li is plated into the porous substrate. Since that Ag-Li alloy is adequately lithiophilic with a high bonding energy to Li, the pre-formed Ag-Li seeds the Li nucleation homogeneously on Ni substrate and guides the Li deposition into 3D porous structure [43, 44]. In this manner, a dendrite-free Li coating layer underneath the dense SEI is formed on the Canvas Ni-Ag_2S electrode, as evidenced by SEM images in **Fig. 3**g-i. This is further confirmed by the cross-sectional SEM observation in **Fig. 3**j-l. The plated Li can be guided into the inner porous structure and homogenously coated on the Ni fibers, since that the Ag-Li is evenly covered on the Ni fibers and

plays a key role of drainage for Li deposition. As a comparison, SEM images (**Fig. 3**m-o) of the Li deposition on a planar Cu foil illustrate needle-like Li dendrites. The dendrites grow vertically on the top of planar Cu foil, posing a huge safety hazard, which may pierce the separator and make a short circuit of the battery at any time. Benefiting from the dendrite-free nature of Canvas Ni-Ag_2S, even after that Li is completely stripped from the electrode, the SEI layer is perfectly remained on the Ni fibers, as shown in **Fig. S12**a. As a comparison, the SEI layer on Canvas Ni is partially destroyed, and it is observed that a small amount of dead Li is remained in the structure (**Fig. S12**b). For Cu foil, a large amount of porous Li clusters are found on the surface after the stripping of Li (**Fig. S13**), indicating that Li@Cu foil anode must have a low Coulombic efficiency (CE).

As-encouraged by the above excellent Li deposition behavior on the Canvas Ni-Ag_2S electrode, the repeated Li plating/stripping performance was further investigated. The CE of different electrodes, as shown in **Fig. S14**a, were measured by assembling Li │Cu Foil, Li │Canvas Ni and Li │Canvas Ni-Ag_2S half-cells, respectively. The CE of Li │Canvas Ni-Ag_2S cell reaches a high value of 98% after several cycles, which can be maintained throughout the entire test upon 150 cycles, exhibiting an outstanding cyclic reversibility. In contrast, Li │Cu foil cell shows a low CE of less than 95%, and because of the uncontrolled dendrite growth, an internal short-circuit can be observed after 60 cycles. In addition, owing to its micro-nano 3D porous structure which can somewhat confine the Li crystals inside the porous structure, Canvas Ni electrode also shows better cycle performance than planar Cu foil. However, since that large dendritic crystals can be still observed in the top surface and the large pores of the Canvas Ni frameworks (**Fig. 3**a,f), the risk of piercing the separator is obvious for the un-modified 3D current collector. The potential profiles of the plating and striping processes at different cycles for these cells are shown in **Fig. S14**b,c,d.

The polarization of Li plating on Canvas Ni-Ag_2S electrode in the 10th, 50th and 100th cycles manifest potentials of -28 mV, -25 mV and -24 mV vs. Li, respectively. The low value of over-potential for Canvas Ni-Ag_2S in the initial cycles confirms that the pre-generated Li_2S SEI owns high ion conductivity. Moreover, benefiting from the dendrite-free characteristic, a stabilized polarization potential of 25 mV suggests that the SEI layer is maintained during repeated plating/stripping. The sudden increase of potential occurs at the end of each stripping step, indicating that the reversible part of Li metal has been completely stripped from the electrode. It can be seen from these profiles that reversible areal capacity of Li is increasing and stabilizing upon cycling for the Canvas Ni-Ag_2S. This phenomenon also demonstrates that the high conductive SEI layer remains stable during cycling.

It is worth pointing out that the half-cell test is generally unable to withstand a large number of cycling due to unsatisfactory cycle performance of Li metal foil used as the counter/reference electrode [45]. In order to further verify the superior cyclic performance of Li on Canvas Ni-Ag_2S electrode, symmetric Li@Canvas Ni-Ag_2S | Li@Canvas Ni-Ag_2S cells were assembled to avoid the instability caused by using Li metal foil. Symmetric cells of bare Li foil and Li@Canvas Ni were also assembled as control groups. Due to that the working electrode and the reference electrode are identical, the voltage hysteresis, namely the offset value between Li stripping and plating, can reasonably reflect the interfacial stability and charge transfer resistance of an electrochemical system at constant current densities. **Fig. 4**a shows the voltage profiles when the cells are running under mutative current densities and capacities. This measurement is useful for simulating the alterable charging/discharging circumstance in actual use. The Li foil | Li foil symmetric cell exhibits a high voltage hysteresis of 40 mV at a current density of 0.1 mA cm^{-2}. After then, a sudden internal short-circuit in the bare Li foil cell occurs when the current density

is increased to 1 mA cm^{-2}. The size and number density of Li nuclei are directly proportional to current density and capacity respectively [18], thereby, both the diameter and number of Li nuclei would show an extremely uneven distribution under variable current densities and capacities, leading to more severe dendrite growth and easy piercing of the separator. Benefiting from the hierarchical micro-nano structure which can effectively decentralize the local current density, Li@Canvas Ni symmetric cell shows lower voltage hysteresis than the Li foil cell, and the voltage hysteresis is even stable and lower for the Li@Canvas Ni-Ag_2S cell.

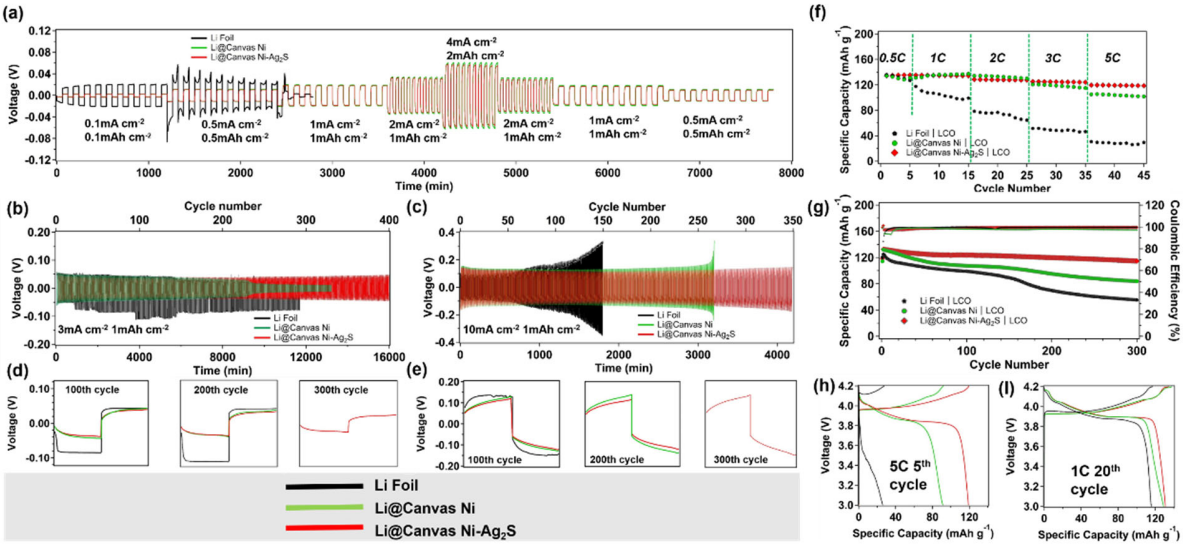

Fig. 4. Electrochemical cycle performance of different electrodes containing Li metal. a, b, c) Voltage profiles of bare Li foil symmetric cells (black), Li@Canvas Ni symmetric cells (green) and Li@Canvas Ni-Ag_2S symmetric cells (red) a) at different current densities with different capacities; b) at 3 mA cm^{-2} with a capacity of 1 mA h cm^{-2} and c) at 10 mA cm^{-2} with a capacity of 1 mA h cm^{-2}, d) shows the zoomed-in voltage profiles at different cycles correspond to (b); e) shows the zoomed-in voltage profiles at different cycles correspond to (c). f) Rate performance and g) long-term cycle performance of full cells using LCO as cathode. Voltage profiles corresponding to Li Foil | LCO full cell (black), Li@Canvas Ni | LCO full cell (green) and Li@Canvas Ni | Ag_2S-LCO full cell (red) at h) 5th cycle with the rate of 5 C and i) 20th cycle with the rate of 1 C.

The voltage profiles of different symmetric cells measured at 3 mA cm^{-2} with a restricted areal capacity of 1 mA h cm^{-2} are shown in **Fig. 4**b. The details of the voltage-time curves at the 100th, 200th and 300th cycles are also captured and exhibited in **Fig. 4**d. In comparison to the high over-potential (>100 mV) presented by bare Li foil symmetric cell, both Li@Canvas Ni and Li@Canvas Ni-Ag_2S exhibit over-potentials lower than 60 mV at the beginning of cycling. Upon cycling, the over-potentials gradually decrease and finally stabilize to around 40 mV. However, after 200 cycles, voltage hysteresis of Li@Canvas Ni cell starts to decrease to an abnormally low value with a flat voltage profile, indicating that a short circuit happens due to the inevitable Li dendrite growth on the un-modified metallic 3D current collector. Significantly, Li@Canvas Ni-Ag_2S cell illustrates stable voltage plateaus even after 300 cycles, demonstrating its superior cycle performance enabled by the uniform deposition of Li as-accelerated by the Ag_2S-induced nuclei. Additionally, the Canvas Ni-Ag_2S electrode can maintain its morphology after 400 cycles (**Fig. S**18), indicating that this kind of electrode owns superior mechanical strength to withstand the volume expansion during cycling. Moreover, to meet the demands of fast charging/discharging, cycle performance of the cells under a high current density of 10 mA cm^{-2} were evaluated, as shown in **Fig. 4**c and **Fig. 4**e. A continuously aggravated polarization of Li plating/stripping on bare Li foil is observed, which is represented by the gradual rising trend of voltage hysteresis that starts from around 50th cycle. As for Li@Canvas Ni cell, this trend is delayed until 150th cycle, confirming that a better performance can be achieved by using 3D current collector. The sharp increase of voltage hysteresis in Li@Canvas Ni cell after 260 cycles is observed, implying that the "electrical disconnection" is the failure mechanism of the cell rather than short circuit. As it is well known that upon cycling some Li fragments may detach from the Li substrate and are wrapped in an electronically insulating SEI coating, thus losing their electrochemical activity, and forming the

so called “Dead Li” [46]. Meanwhile, a porous and high impedance interphase will be formed on Li metal surface due to the formation of “Dead Li”. This is especially serious when the cell is tested at high current density, appearing as the aggravated polarization in the voltage profiles [45]. As for the Li@Canvas Ni-Ag_2S symmetric cell, an alleviated polarization is observed. The hysteresis voltage increases from 240 mV at the 100th cycle to 270 mV at the 300th cycle. Another noteworthy point is the shape of voltage-time curve in each cycle which exhibits a well-defined plateau with smooth upward tilting, indicating the uniform Li plating/stripping behavior for Li@Canvas Ni-Ag_2S electrode [47]. In comparison, the “arch” voltage curve is observed for Li foil cell, indicating that a porous structure is formed on Li foil caused by the formation of “Dead Li”, leading to the non-uniform plating/stripping kinetics on the porous surface.

Combining $LiCoO_2$ (LCO) cathode with Li metal anodes for evaluating the actual performance in full cells, Li@Canvas Ni │LCO, Li@Canvas Ni-Ag_2S │LCO and Li foil │LCO batteries were assembled with traditional binary carbonate electrolyte and the galvanostatic charge/discharge test was conducted. As shown in **Fig. 4**f, Li@Canvas Ni-Ag_2S │LCO exhibits prominent advantages in rate performance, which displays a high discharge capacity of 139 mA h g^{-1} at 1 C and a satisfying value of 120 mA h g^{-1} at 5 C, however the discharge capacities of the Li@Canvas Ni │LCO and Li foil │LCO batteries show lower values of 92 mA h g^{-1} and 28 mA h g^{-1}, respectively. Severe polarization is observed in the charging/discharging voltage curve of Li foil │LCO battery as shown in **Fig. 4**h, which can be ascribed to the sluggish Li^+ transmission at high current density. **Fig. 4**g,l shows the long-term cycle performance at 1 C. The Li@Canvas Ni-Ag_2S │LCO battery displays an initial capacity of 136 mA h g^{-1}, and the value is slightly decreased to 126 mA h g^{-1} after 20 cycles due to the process of SEI formation. 96.8% of the initial capacity can be reserved after 300 cycles with a value of 122 mA h g^{-1}. Moreover, a high CE over 99.9% is

observed throughout the entire testing stage. As a comparison, the capacities for the Li@Canvas Ni | LCO and Li foil | LCO batteries decrease severely, especially for the Li foil battery. The superior cyclic stability for the Li@Canvas Ni-Ag_2S | LCO battery can be mainly explained by two reasons: i) The pre-generated Li_2S serves as the SEI layer which can mitigate the consumption of electrolyte for generating SEI in the binary carbonate electrolyte. As a contrast, the SEI formation process in Li@Canvas Ni | LCO lasts for a long period, which can be evidenced by the continuous loss of discharge capacity during the initial 100 cycles. ii) The dendrite-free surface can protect the as-generated SEI layer from repeated destruction and regeneration. In contrast, Li foil | LCO battery shows continuous fading of capacity from the initial 125 mA h g^{-1} to the final 48 mA h g^{-1} due to the unceasing renovation of SEI.

The effective principle of Canvas Ni-Ag_2S electrode is depicted in detail in **Fig. 5**a. It is well known that electrolyte is consumed in electrochemical cycle as SEI formation [48]. As confirmed hereinbefore, when dendritic Li is repeatedly formed on the top of a un-modified 3D current collector (Canvas Ni), SEI layer with a low shear modulus experiences incessant destruction and reparation [49], finally resulting in depletion of electrolyte, formation of an ultra-thick SEI layer and creation of large "dead Li". However, by introducing Ag_2S NPs onto the 3D current collector, Li^+ can be transported towards inner surface of 3D framework and deposited inside the framework, forming a dendrite-free morphology. Hence, the thickening of SEI and "Dead Li" layer can be greatly alleviated, guaranteeing a high cyclic stability of battery. [15, 50]

Electrochemical impedance spectroscopy (EIS) was conducted with different symmetric cells to support these viewpoints, with the spectra shown in **Fig. 5**b-d. The equivalent circuit for fitting the EIS curves is shown in **Fig. 5**e. Here, R_s refers to the electrolyte ohmic resistance, and Z_w denotes Warburg resistance sourcing from the diffusion process of Li^+ in the bulk of electrode;

428 R_{CT} and R_{SEI} represent resistances of charge transfer process and SEI, respectively; C_{CT} and C_{SEI}
429 are two constant phase elements of electrode and SEI film respectively. The enlarged polarization
430 on the surface of electrodes during cycling significantly influence the value of R_{SEI}, which can be
431 used for evaluating the impedance caused by thickening of SEI and accumulation of "Dead Li".
432 As shown in **Fig. 5**f, R_{SEI} value of the bare Canvas Ni-Ag_2S electrode is 127.9 Ω for the fresh cell
433 and values at the 50th and 150th cycles are 2.1 and 14.99 Ω, while these values for Canvas Ni are
434 97.6, 5.8, and 56.3 Ω, respectively. The rapid decrease in R_{SEI} after cycling demonstrates the
435 formation of the SEI layer that provides an efficient Li^+ transfer pathway. Benefiting from the
436 micro-nano structure of Canvas Ni framework, electrolyte is able to contact the active sites
437 sufficiently, leading to a further reduction of R_{SEI} in Canvas Ni and Canvas Ni-Ag_2S as compared
438 with the Li foil. Moreover, the conversion of Ag_2S to metallic Ag can somewhat increase electronic
439 conductivity of Canvas Ni-Ag_2S electrode. Therefore, both the Canvas Ni-Ag_2S and the Canvas
440 Ni showed low R_{SEI} value after 50 cycles. But when the number of cycles is increased to 150, R_{SEI}
441 value of Canvas Ni electrode gradually increased to 56.3 Ω, revealing a severe deterioration of
442 cyclic stability. Meanwhile, R_{SEI} value of Canvas Ni-Ag_2S remains stable for the following cycles,
443 confirming the effectiveness of Canvas Ni-Ag_2S electrode for enhancing cyclic stability of Li
444 metal anode as we depicted hereinbefore. The SEM images after 150 cycles that are shown in **Fig.**
445 **5**a, providing the evidence for the above description. As for the Canvas Ni electrode after EIS
446 measurement, large "Dead Li" agglomerate and fractured SEI can be observed on the surface. The
447 uneven and porous surface leads to non-uniform electrochemical kinetics and high impedance.
448 However, even after a long-term cycling, on the Canvas Ni-Ag_2S electrode, metallic Li is still
449 evenly located underneath the SEI, and the well-preserved electrode without damage can be clearly
450 observed. All of these strongly demonstrate that the Canvas Ni-Ag_2S electrode can significantly

enhance the cyclic stability of Li metal anode. Table S2 shows the comparison with the recent frontier reports.

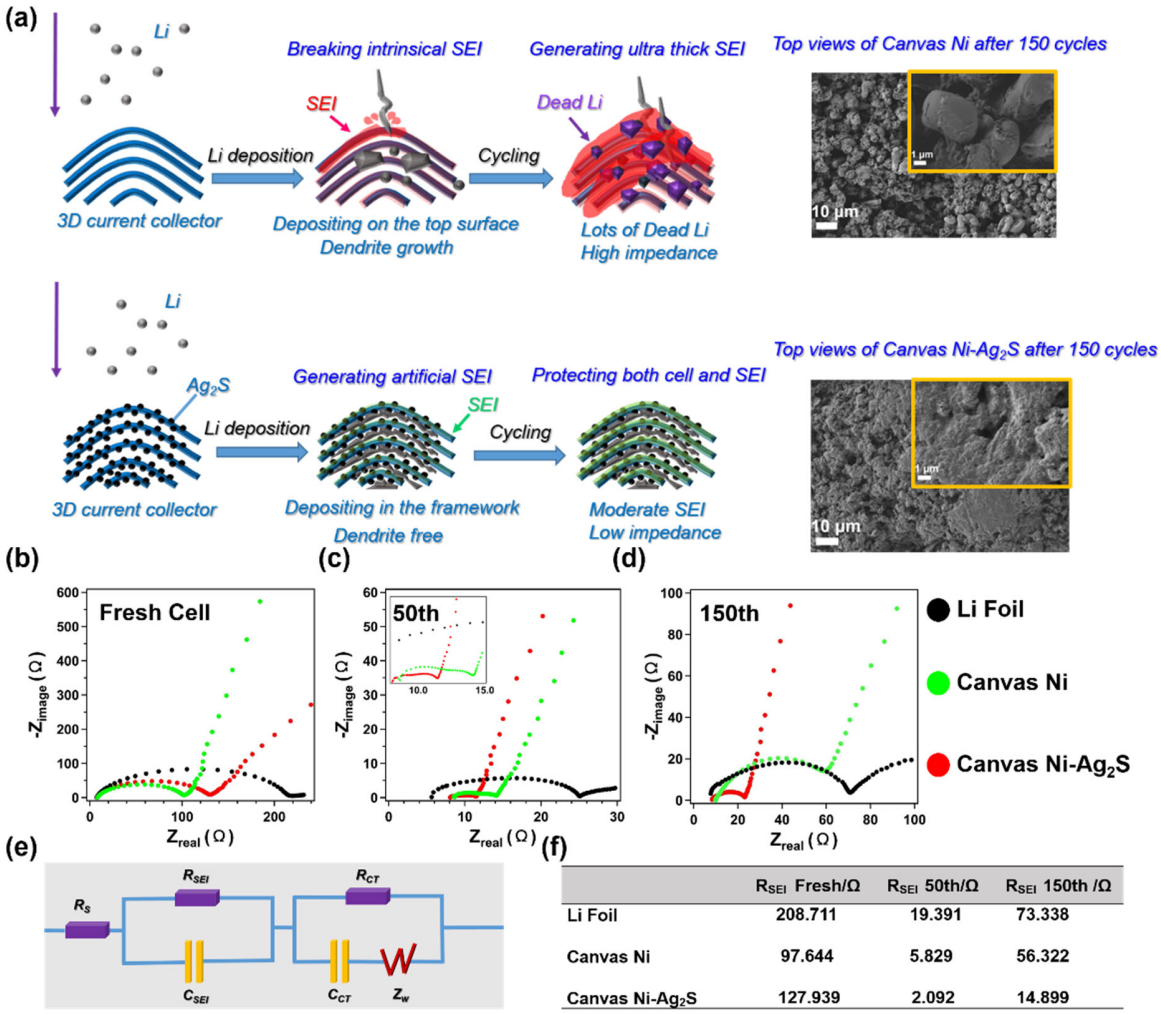

	R_{SEI} Fresh/Ω	R_{SEI} 50th/Ω	R_{SEI} 150th /Ω
Li Foil	208.711	19.391	73.338
Canvas Ni	97.644	5.829	56.322
Canvas Ni-Ag_2S	127.939	2.092	14.899

Fig. 5. (a) Schematic diagram of the multifaceted cycle performance degradation when Li repeatedly plating/ stripping on a common 3D current collector (top), and the enhanced stable cycle performance of the Canvas Ni-Ag2S (below); morphologies of the electrodes after 150 cycles are included as illustrations. The comparison of EIS of different electrodes (b) be fore cycling, (c) after 50 cycles and (d) after 150 cycles. (e) The corresponding equivalent circuit drawn for simulating EIS curves. (f) The SEI resistance of different electrodes after different cycles. Results were obtained from symmetric cells measurement at 1 mA cm^{-2} with cycling capacity of 1 mA h cm^{-2}.

4. Conclusion

In summary, we have fabricated a canvas textile structured Ni current collector for Li metal anode and a new method for promoting uniform electrodeposition of Li metal into 3D current collector by decorating with Ag_2S was introduced. The Canvas Ni 3D current collector whose structure was inspired by cotton textile fabric showed a unique hierarchical micro-nano structure, by which the local current density could be reduced and Li metal could be accommodated becomingly. Moreover, through a modified silver-mirror reaction, Ag_2S NPs were uniformly decorated on Canvas Ni, which offered nucleation sites for Li metal and surface-covered Li_2S pre-SEI. Our Ag_2S-decorated and textile-structured Canvas Ni 3D current collector presented obvious advantages compared to conventional 3D current collector, such as smooth and homogenous Li deposition, stabilized SEI, reduced over-potential and alleviated polarization. Beneficial from these characteristics, the Canvas Ni-Ag_2S electrode showed high CE of 98%, low voltage hysteresis during cycling, superior cyclic stability at high current densities, *i.e.,* up to 400 cycles at 3 mA cm^{-2}, 1 mA h cm^{-2} and 350 cycles at 10 mA cm^{-2}, 1 mA h cm^{-2}. When Li@Canvas Ni-Ag_2S was used as the anode in Li │ LCO battery, high CE (>99.9%), long lifespan (90.4% capacity was remained after 300 cycles) and high rate capability (120 mA h g^{-1} at 5 C) were achieved. All of those reinforced that our new 3D current collector could be applied to Li metal anode. Furthermore, this paper also presents a new method for preparing textile metallic framework with a unique porous structure which has never been reported, and we anticipate that many studies requiring the use of bio-structured metals would benefit from this work.

494

495

496 **Appendix A.**

497 Supplementary data

498

499 **REFERENCES**

500 [1] L. Liu, Y. X. Yin, J.Y. Li, N.W. Li, X.X. Zeng, H. Ye, Y. G. Guo, L. J. Wan, Free-Standing
501 Hollow Carbon Fibers as High-Capacity Containers for Stable Lithium Metal Anodes, Joule 1
502 (2017) 563-575.

503 [2] P. G. Bruce, S. A. Freunberger, L. J. Hardwick, J-M. Tarascon, Li-O_2 and Li-S batteries with
504 high energy storage, Nat. Mater. 11 (2012) 19-29.

505 [3] W. Xu, J. Wang, F. Ding, X. Chen, E. Nasybulin, Y. Zhang, J-G. Zhang, Lithium metal anodes
506 for rechargeable batteries, Energy Environ. Sci. 7 (2014) 513-537.

507 [4] D. Aurbach, E. Zinigrad, Y. Cohen and H. Teller, A short review of failure mechanisms of
508 lithium metal and lithiated graphite anodes in liquid electrolyte solutions, Solid State Ionics 148
509 (2002) 405-416.

510 [5] S. Huang, L. Tang, H. S. Najafabadi, S. Chen, Z. Ren, A highly flexible semi-tubular carbon
511 film for stable lithium metal anodes in high-performance batteries, Nano Energy 38 (2017) 504-
512 509.

513 [6] R. Xu, X. Q. Zhang, X. B. C, H. J. Peng, C. Z. Zhao, C. Yan, J. Q. Huang, Artificial Soft-Rigid
514 Protective Layer for Dendrite-Free Lithium Metal Anode, Adv. Funct. Mater. 28 (2018) 1705838.

515 [7] Y. Liu, D. Lin, P. Y. Yuen, K. Liu, J. Xie, R. H. Dauskardt, Y. Cui, An Artificial Solid
516 Electrolyte Interphase with High Li-Ion Conductivity, Mechanical Strength, and Flexibility for
517 Stable Lithium Metal Anodes, Adv. Mater. 29 (2017) 1605531.

518 [8] N. W. Li, Y. X. Yin, C. P. Yang, Y. G. Guo, An Artificial Solid Electrolyte Interphase Layer
519 for Stable Lithium Metal Anodes, Adv. Mater. 28 (2016) 1853-1858.

520 [9] K. Yan, H. W. Lee, T. Gao, G. Zheng, H. Yao, H. Wang, Z. Lu, Y. Zhou, Z. Liang, Z. Liu, S.
521 Chu, Y. Cui, Ultrathin two-dimensional atomic crystals as stable interfacial layer for improvement
522 of lithium metal anode, Nano Lett. 14 (2014) 6016-6022.

523 [10] C. Huang, J. Xiao, Y. Shao, J. Zheng, W. D. Bennett, D. Lu, L. V. Saraf, M. Engelhard, L. Ji,
524 J. Zhang, X. Li, G. L. Graff, J. Liu, Manipulating surface reactions in lithium-sulphur batteries
525 using hybrid anode structures, Nat. Commun. 5 (2014) 3015.

526 [11] H. Chen, A. Pei, D. Lin, J. Xie, A. Yang, J. Xu, K. Lin, J. Wang, H. Wang, F. Shi, D. Boyle,
527 Y. Cui, Uniform High Ionic Conducting Lithium Sulfide Protection Layer for Stable Lithium
528 Metal Anode, Adv. Energy Mater. 9 (2019) 1900858.

529 [12] Y. Yuan, F. Wu, Y. Bai, Y. Li, G. Chen, Z. Wang, C. Wu, Regulating Li deposition by
530 constructing LiF-rich host for dendrite-free lithium metal anode, Energy Storage Materials 16
531 (2019) 411-418.

[13] Y. Yuan, F. Wu, G. Chen, Y. Bai, C. Wu, Porous LiF layer fabricated by a facile chemical method toward dendrite-free lithium metal anode, Journal of Energy Chemistry 37 (2019) 197-203.

[14] X. B. Cheng, Q. Zhang, J. Mater. Chem. A. Dendrite-free lithium metal anodes: stable solid electrolyte interphases for high-efficiency batteries, 3 (2015) 7207-7209.

[15] X. B. Cheng, R. Zhang, C. Z. Zhao, Q. Zhang, Toward Safe Lithium Metal Anode in Rechargeable Batteries: A Review, Chem. Rev. 117 (2017) 10403-10473.

[16] C. Brissot, M. Rosso, J. N. Chazalviel, P. Baudry, S. Lascaud, In situ study of dendritic growth in lithium/PEO-salt/lithium cells, Electrochimica Acta 43 (1998) 1569-1574.

[17] R. Zhang, X. R. Chen, X. Chen, X. B. Cheng, X. Q. Zhang, C. Yan, Q. Zhang, Lithiophilic Sites in Doped Graphene Guide Uniform Lithium Nucleation for Dendrite-Free Lithium Metal Anodes, Angew. Chem. Int. Ed. Engl. 56 (2017) 7764-7768.

[18] A. Pei, G. Zheng, F. Shi, Y. Li, Y. Cui, Nanoscale Nucleation and Growth of Electrodeposited Lithium Metal, Nano Lett.17 (2017) 1132-1139.

[19] F. Wu, Y-X. Yuan, X-B. Cheng, Y. Bai, Y. Li, C. Wu, Q. Zhang, Perspectives for restraining harsh lithium dendrite growth: Towards robust lithium metal anodes Energy Storage Materials 15 (2018) 148-170.

[20] L. L. Lu, J. Ge, J. N. Yang, S. M. Chen, H. B. Yao, F. Zhou, S. H. Yu, Free-Standing Copper Nanowire Network Current Collector for Improving Lithium Anode Performance, Nano Lett. 16 (2016) 4431-4437.

[21] Q. Li, S. Zhu, Y. Lu, 3D Porous Cu Current Collector/Li-Metal Composite Anode for Stable Lithium-Metal Batteries, Adv. Funct. Mater. 27 (2017) 1606422.

[22] Y. Zhang, C. Wang, G. Pastel, Y. Kuang, H. Xie, Y. Li, B. Liu, W. Luo, C. Chen, L. Hu, 3D Wettable Framework for Dendrite-Free Alkali Metal Anodes, Adv. Energy. Mater. 8 (2018) 1800635.

[23] C. Jin, O. Sheng, Y. Lu, J. Luo, H. Yuan, W. Zhang, H. Huang, Y. Gan, Y. Xia, C. Liang, J. Zhang, X. Tao, Metal oxide nanoparticles induced step-edge nucleation of stable Li metal anode working under an ultrahigh current density of 15 mA cm^{-2}, Nano Energy 45 (2018) 203-209.

[24] S. Huang, W. Zhang, H. Ming, G. Cao, L-Z. Fan, H. Zhang, Chemical Energy Release Driven Lithiophilic Layer on 1 m^2 Commercial Brass Mesh toward Highly Stable Lithium Metal Batteries, Nano. Lett. 19 (2019) 832-1837.

[25] H. Yang, C. Guo, A. Naveed, J. Lei, J. Yang, Y. Nuli, J. Wang, Recent progress and perspective on lithium metal anode protection, Energy Storage Materials 14 (2018) 199-221

[26] C. P. Yang, Y. X. Yin, S. F. Zhang, N. W. Li, Y. G. Guo, Accommodating lithium into 3D current collectors with a submicron skeleton towards long-life lithium metal anodes, Nat. Commun. 6 (2015) 8058.

569 [27] Y. Wang, Z. Wang, D. Lei, W. Lv, Q. Zhao, B. Ni, Y. Liu, B. Li, F. Kang, Y. B. He, Spherical
570 Li Deposited inside 3D Cu Skeleton as Anode with Ultrastable Performance, ACS Appl. Mater.
571 Interfaces 10 (2018) 20244-20249.

572 [28] Q. Yun, Y. B. He, W. Lv, Y. Zhao, B. Li, F. Kang, Q. H. Yang, Chemical Dealloying Derived
573 3D Porous Current Collector for Li Metal Anodes, Adv. Mater. 28 (2016) 6932-6939.

574 [29] Y. An, H. Fei, G. Zeng, X. Xu, L. Ci, B. Xi, S. Xiong, J. Feng, Y. Qian, Vacuum distillation
575 derived 3D porous current collector for stable lithium–metal batteries, Nano Energy 47 (2018)
576 503-511.

577 [30] H. Zhao, D. Lei, Y. B. He, Y. Yuan, Q. Yun, B. Ni, W. Lv, B. Li, Q. H. Yang, F. Kang, J. Lu,
578 Compact 3D Copper with Uniform Porous Structure Derived by Electrochemical Dealloying as
579 Dendrite-Free Lithium Metal Anode Current Collector, Adv. Energy Mater. 8 (2018) 1800266.

580 [31] S. S. Chi, Y. Liu, W. L. Song, L. Z. Fan, Q. Zhang, Prestoring Lithium into Stable 3D Nickel
581 Foam Host as Dendrite-Free Lithium Metal Anode, Adv. Funct. Mater. 27 (2017) 1700348.

582 [32] J. Zhu, J. Chen, Y. Luo, S. Sun, L. Qin, H. Xu, P. Zhang, W. Zhang, W. Tian, Z. Sun,
583 Lithiophilic metallic nitrides modified nickel foam by plasma for stable lithium metal anode,
584 Energy Storage Materials 23 (2019) 539-546.

585 [33] S. Wu, Z. Zhang, M. Lan, S. Yang, J. Cheng, J. Cai, J. Shen, Y. Zhu, K. Zhang, W. Zhang,
586 Lithiophilic Cu-CuO-Ni Hybrid Structure: Advanced Current Collectors Toward Stable Lithium
587 Metal Anodes, Adv. Mater. 30 (2018) 1705830.

588 [34] B-H. Hou, Y-Y. Wang, Q-L. Ning, W-H. Li, X-T. Xi, X. Yang, H-J. Liang, X. Feng, X-L.
589 Wu, Self-Supporting, Flexible, Additive-Free, and Scalable Hard Carbon Paper Self-Interwoven

by 1D Microbelts: Superb Room/Low-Temperature Sodium Storage and Working Mechanism, Adv. Mater. (2019) 1903125.

[35] J. Gao, X. Cai, J. Wang, M. Hou, L. Lai, L. Zhang, Recent progress in hierarchically structured O_2-cathodes for Li-O2 batteries, Chemical Engineering Journal 352 (2018) 972-995.

[36] Y. Ouyang, X. Xia, H. Ye, L. Wang, X. Jiao, W. Lei, Q. Hao, Three-Dimensional Hierarchical Structure ZnO@C@NiO on Carbon Cloth for Asymmetric Supercapacitor with Enhanced Cycle Stability, ACS Appl. Mater. Interfaces 10 (2018) 3549-3561.

[37] X. Xie, L. Hu, M. Pasta, G. F. Wells, D. Kong, C. S. Criddle, Y. Cui, Three-dimensional carbon nanotube-textile anode for high-performance microbial fuel cells, Nano Lett. 11 (2011) 291-296.

[38] L-L. Lu, Y-Y. Lu, Z-J. Xiao, T-W. Zhang, F. Zhou, T. Ma, Y. Ning, H-B. Yao, S-H. Yu, Y. Cui, Wood-Inspired High-Performance Ultrathick Bulk Battery Electrodes, Adv. Mater. 30 (2018) 1706745.

[39] L. Qu, L. Dai, Novel silver nanostructures from silver mirror reaction on reactive substrates, J. Phys. Chem. B. 109 (2005) 13985-13990.

[40] A. Kushima, K. P. So, C. Su, P. Bai, N. Kuriyama, T. Maebashi, Y. Fujiwara, M. Z. Bazant, J. Li, Liquid cell transmission electron microscopy observation of lithium metal growth and dissolution: Root growth, dead lithium and lithium flotsams, Nano Energy 32 (2017) 271-279.

[41] P. Barai, K. Higa, V. Srinivasan, Effect of Initial State of Lithium on the Propensity for Dendrite Formation: A Theoretical Study, Journal of The Electrochemical Society 164 (2016) A180-A189.

[42] X-B. Cheng, C. Yan, H-J. Peng, J-Q. Huang, S-T. Yang, Q. Zhang, Sulfurized solid electrolyte interphases with a rapid Li^+ diffusion on dendrite-free Li metal anodes Energy Storage Materials 10 (2018) 199-205.

[43] C. Yang, Y. Yao, S. He, H. Xie, E. Hitz, L. Hu, Ultrafine Silver Nanoparticles for Seeded Lithium Deposition toward Stable Lithium Metal Anode, Adv. Mater. 29 (2017) 1702714.

[44] R. Zhang, X. Chen, X. Shen, X. Q. Zhang, X. R. Chen, X. B. Cheng, C. Yan, C. Z. Zhao, Q. Zhang, Coralloid Carbon Fiber-Based Composite Lithium Anode for Robust Lithium Metal Batteries, Joule 2 (2018) 764-777.

[45] D. Lu, Y. Shao, T. Lozano, W. D. Bennett, G. L. Graff, B. Polzin, J. Zhang, M. H. Engelhard, N. T. Saenz, W. A. Henderson, P. Bhattacharya, J. Liu, J. Xiao, Failure Mechanism for Fast-Charged Lithium Metal Batteries with Liquid Electrolytes, Adv. Energy Mater. 5 (2015) 1400993.

[46] J. Yamaki, S. Tobishima, K. Hayashi, K. Saito, Y. Nemoto, M. Arakawa, A consideration of the morphology of electrochemically deposited lithium in an organic electrolyte, J. Power Sources 74 (1998) 219-227.

[47] C. Niu, H. Pan, W. Xu, J. Xiao, J. G. Zhang, L. Luo, C. Wang, D. Mei, J. Meng, X. Wang, Z. Liu, L. Mai, J. Liu, Self-smoothing anode for achieving high-energy lithium metal batteries under realistic conditions, Nat. Nanotechnol. 14 (2019) 594-601.

[48] R. Jung, M. Metzger, D. Haering, S. Solchenbach, C. Marino, N. Tsiouvaras, C. Stinner, H. A. Gasteiger, Consumption of Fluoroethylene Carbonate (FEC) on Si-C Composite Electrodes for Li-Ion Batteries, Journal of The Electrochemical Society 163 (2016) A1705-A1716.

631 [49] C. Monroe, J. Newman, The Impact of Elastic Deformation on Deposition Kinetics at
632 Lithium/Polymer Interfaces, Journal of The Electrochemical Society 152 (2005) A396-A404.

633 [50] P. Shi, X-B. Cheng, T. Li, R. Zhang, H. Liu, C. Yan, X-Q. Zhang, J-Q. Huang, Q. Zhang,
634 Electrochemical Diagram of an Ultrathin Lithium Metal Anode in Pouch Cells, Adv. Mater. 31
635 (2019) 1902785.